Simulation of near-infrared photodiode detectors based on β-$FeSi_2$/4H-SiC heterojunctions*

Pu Hong-Bin(蒲红斌)†, He Xin(贺 欣), Quan Ru-Dai(全汝岱), Cao Lin(曹 琳), and Chen Zhi-Ming(陈治明)

Department of Electronic Engineering, Xi'an University of Technology, Xi'an 710048, *China*

(Received 20 April 2012; revised manuscript received 30 August 2012)

In this paper, we propose a near-infrared p-type β-$FeSi_2$/n-type 4H-SiC heterojunction photodetector with semiconducting silicide (β-$FeSi_2$) as the active region for the first time. The optoelectronic characteristics of the photodetector are simulated using a commercial simulator at room temperature. The results show that the photodetector has a good rectifying character and a good response to near-infrared light. Interface states should be minimized to obtain a lower reverse leakage current. The response spectrum of the β-$FeSi_2$/4H-SiC detector, which consists of a p-type β-$FeSi_2$ absorption layer with a doping concentration of 1×10^{15} cm^{-3} and a thickness of 2.5 μm, has a peak of 755 mA/W at 1.42 μm. The illumination of the SiC side obtains a higher responsivity than that of the β-$FeSi_2$ side. The results illustrate that the β-$FeSi_2$/4H-SiC heterojunction can be used as a near-infrared photodetector compatible with near-infrared optically-activated SiC-based power switching devices.

Keywords: β-$FeSi_2$/4H-SiC, near-infrared photodetector, spectral response

PACS: 73.40.Lq, 85.60.Dw, 71.15.Pd, 61.43.Dq **DOI:** 10.1088/1674-1056/22/3/037301

1. Introduction

Currently, the majority of optical fiber transmission systems operate at wavelengths of 1.3 and 1.55 μm in order to take advantage of the low-loss and low-dispersion characteristics of silica-based optical fibers at these wavelengths. Therefore, extraordinary technological innovations are increasingly adopted within the telecommunication industry as a means of developing optoelectronic devices which operate in the near-infrared (NIR) region.

Semiconducting orthorhombic iron disilicide (β-$FeSi_2$) is one of the best candidates for NIR photodetection owing to its unique properties: a direct optical band gap of 0.85 eV, and a relatively large optical absorption coefficient that exceeds 10^5 cm^{-1} at 1.2 eV. Furthermore, thin films of β-$FeSi_2$ can be easily grown on almost any solid-state substrate, such as Si,[1] InP,[2] GaAs,[3] 3C-SiC,[4] SiO_2,[5] 7059 glass,[6] stainless steel,[7] and sapphire.[8] More importantly, β-$FeSi_2$ is an ecologically friendly material due to the non-toxicity of the elements (Fe and Si) and their abundance in the Earth's crust.

Recently, β-$FeSi_2$/Si pn photodetectors (PDs) with β-$FeSi_2$ thin films deposited on Si wafer were fabricated by several groups,[9–11] and showed good rectifying properties and light detection ability in the NIR region. Various deposition methods such as ion beam synthesis, reactive deposition epitaxy, sputtering, and molecular beam epitaxy have been adopted for the growth of β-$FeSi_2$. However, most of these methods generally require thermal treatments at temperature higher than 800 °C after the film deposition, which actively causes a diffusion of the Fe atoms from the β-$FeSi_2$ layer to the Si layer during the film preparation. The Fe atoms migrate into a depletion layer within Si, which leads to interface defects, produces a leakage current, and forms trap centers for photogenerate carriers.[9] To overcome this problem, n-type β-$FeSi_2$/i-Si/p-type Si photodetectors[10] can be obtained with a lower leakage current than that of the n-type β-$FeSi_2$/p-type Si.[9]

We are interested in the SiC-based heterojunction because of its potential application in optoelectronics and power electronics fields, including light sensors and light-activated high-power switching devices to be used at high temperature. As a result, silicon devices cannot effectively fulfill all the tasks. Unfortunately, SiC is transparent to most visible light and all infrared (IR) light. Thus, PDs and other photoelectric devices made of SiC are not sensitive to either GaAs based lasers or the other existing light sources that typically work in the IR region. In order to make SiC-based IR PDs, we can adopt a heterojunction structure.[12] However, earlier work on SiC IR PDs has focused primarily on SiCGe/SiC and Si/SiC heterojunction devices. The choice of indirect band gapped SiCGe or Si material has been motivated by its narrower energy gap, and a series of works have been done to grow ternary alloy SiCGe or monocrystalline Si on SiC substrates using the hot-wall chemical vapor deposition (HWCVD) method.[13,14] However, the spectral responses of the SiCGe/SiC and Si/SiC PDs are still weak.[15] This is perhaps because that the SiCGe or Si material has a low optical absorption coefficient and the presence of interface traps can seriously degrade the characteristics of PDs.[16] As we have proposed, a promising way to solve this problem is to adopt a β-$FeSi_2$/4H-SiC pn heterojunction structure, in which the p-type β-$FeSi_2$ is used as a light-absorption

*Project supported by the National Natural Science Foundation of China (Grant Nos. 60876050 and 51177134).

†Corresponding author. E-mail: puhongbin@xaut.edu.cn

© 2013 Chinese Physical Society and IOP Publishing Ltd

layer due to its higher optical absorption coefficient, and is grown on a n^+-type 4H-SiC substrate covered with a thin layer of n-type 4H-SiC epilayer. Up to now, there is only one report of the growth of epitaxial β-$FeSi_2$ thin film on a 3C-SiC buffer layer on a Si substrate. The β-$FeSi_2$ films (150-nm thick) have been successfully deposited on 3C-SiC by co-sputtering iron and silicon in an argon atmosphere.[4] The full-width at half maximum of the rocking curve of the β-$FeSi_2$ 800 diffraction peaks was 1.8°.

In SiC, the diffusion coefficients of Fe atoms are much lower than those in Si. Compared with the β-$FeSi_2$/Si heterojunction PD, the β-$FeSi_2$/SiC heterojunction PD can have a lower leakage current and a better response, and the Fe atoms from the β-$FeSi_2$ layer can hardly diffuse into the SiC layer during the film preparation of the high-temperature thermal treatment.[17] Until now, there are no reports on the investigation of the optoelectronic characteristics of the β-$FeSi_2$/SiC heterojunction.

The purpose of this work is to propose a p-type β-$FeSi_2$/n-type 4H-SiC heterojunction that can be used as an NIR PD. Employing a two-dimensional (2D) physically based device simulator, SILVACO,[18] the structural and optoelectronic characteristics of this novel device are investigated on the basis of the preliminary results about the device structure, numerical modeling, current–voltage (I–V), and photoresponse.

2. Device structure and principle of operation

Like Si-based devices, SiC is also a photosensitive material that enables the development of optically-activated SiC devices, but is transparent to all of the IR regions of the optical spectrum. In order to make a 4H-SiC-based optically controlled device that can be trigged directly by an NIR light source, we propose here a p-type β-$FeSi_2$/n-type 4H-SiC heterojunction PD. A cross-section view of the implemented device is shown in Fig. 1. The device has only two electrodes, i.e., anode and cathode. The starting material is a lightly doped n-type 4H-SiC epilayer grown on n^+-type 4H-SiC substrate. The p-type β-$FeSi_2$ layer designed to act as the activated absorption region can be deposited by means of sputtering using $FeSi_2$ alloy targets with the atomic ratio of Fe:Si=1:2. The p-type β-$FeSi_2$/n-type 4H-SiC heterojunction can be used as a pn PD.

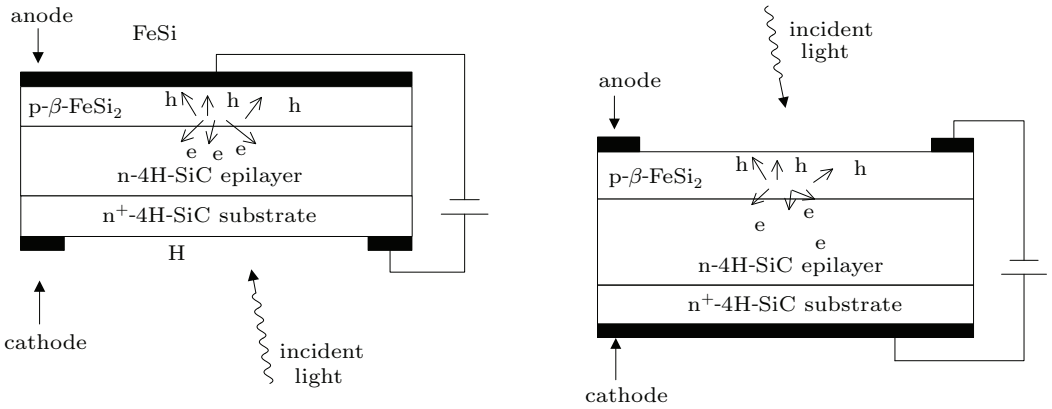


Fig. 1. Schematic structure of p-type β-$FeSi_2$/n-type 4H-SiC PDs.

When the incident light is introduced to the p-type β-$FeSi_2$ activated absorption region of the device from the window at the bottom or on the top, the β-$FeSi_2$ layer will absorb the incident light, and a lot of photogenerated electron hole pairs (EHPs) can be excited through band-to-band transitions. On the reverse-bias voltage, the field in the space-charge layer (SCL) then drives the EHPs in the β-$FeSi_2$ layer to drift towards the n-type 4H-SiC side and the p-type β-$FeSi_2$ side, respectively, and gives rise to an external photocurrent.

For a feasibility study of the β-$FeSi_2$/4H-SiC pn PD, we choose the 2.0-μm n-type 4H-SiC epilayer as the n-type region with the donor concentration of 1.0×10^{16} cm^{-3}. The nominal thickness and the doping concentration of the p-type β-$FeSi_2$ region are 0.8 μm and 1.0×10^{16} cm^{-3}, respectively. According to the parameters of β-$FeSi_2$ and 4H-SiC in literatures, the energy band diagram of the p-type β-$FeSi_2$/n-type 4H-SiC heterojunction is shown in Fig. 2. Here, the electron affinity of β-$FeSi_2$ and 4H-SiC are 3.86 eV and 3.9 eV, respectively.

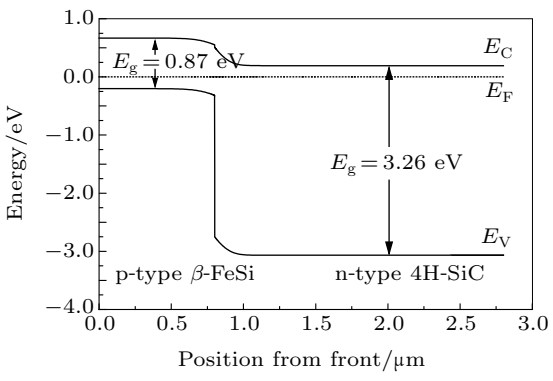


Fig. 2. Energy band diagram of the p-type β-$FeSi_2$/n-type 4H-SiC heterojunction.

3. Numerical modeling

In order to achieve reliable results, it is also necessary to use proper device models for β-$FeSi_2$ material. Several important material parameters used in the simulator have been adjusted to approach published material data of 4H-SiC and β-$FeSi_2$.

3.1. Basic parameters of β-$FeSi_2$ and 4H-SiC layers

In this work, the initial material parameters are selected based on data reported in previous literatures.[19,20] The basic semiconductor properties of the β-$FeSi_2$ and 4H-SiC layers for the simulation are shown in Table 1.

Table 1. Basic parameters used in the simulation for β-$FeSi_2$ and 4H-SiC layers at 300 K.

Parameters	β-$FeSi_2$	4H-SiC
Relative permittivity	22.5	9.7
Acceptor and donor concentration/ cm^{-3}	1×10^{16}	1×10^{16}
Bandgap/eV	0.87	3.26
Effective conduction band density/ cm^{-3}	5.6×10^{19}	1.7×10^{19}
Effective valence band density/ cm^{-3}	2.08×10^{19}	2.5×10^{19}
Electron affinity/eV	3.86	3.90
Ionization energy for donor and acceptor/eV	0.03,0.03	0.06,0.19

3.2. Low-field mobility

Low-field mobility is one of the most important models employed in the device simulation. The SILVACO has developed many low-field mobility models,[18] and the Caughey–Thomas low-field mobility model is chosen for this work. The adjustable low-field mobility is given by

$$\mu_{<\mathrm{n,p}>}(N)=\mu_{\min,<\mathrm{n,p}>}+\frac{\mu_{\max,<\mathrm{n,p}>}-\mu_{\min,<\mathrm{n,p}>}}{1+(N_{<\mathrm{A.D}>}/N_{\mathrm{ref},<\mathrm{n,p}>})^{\phi_{<\mathrm{n,p}>}}},\quad(1)$$

where the carrier mobility $\mu_{<\mathrm{n,p}>}$ is taken as a function of the doping concentration $N_{<\mathrm{A,D}>}$ at 300 K, $\mu_{\max}$, $\mu_{\min}$, N_{ref}, and ϕ are related fitting parameters. The experimental data of mobility for β-$FeSi_2$ and 4H-SiC are taken from Refs. [21] and [22], and the corresponding parameters are listed in Table 2.

Table 2. Fitting parameters of the Caughey-Thomas mobility model for β-$FeSi_2$ and 4H-SiC at 300 K.

Materials	Carriers	$\mu_{\max}/cm^2\cdot V^{-1}\cdot s^{-1}$	$\mu_{\min}/cm^2\cdot V^{-1}\cdot s^{-1}$	$N_{\mathrm{ref}}/10^{17}$ cm^{-3}	ϕ
$\beta-FeSi_2$	Electron	515	2	0.8	0.93
	Hole	256	0.5	1.2	0.82
4H-SiC	Electron	947	0	1.94	0.61
	Hole	124	15.9	176	0.34

3.3. Optical absorption and electron–hole generation rate of the β-$FeSi_2$ layer

To numerically calculate the photocurrent of the β-$FeSi_2$/4H-SiC PD due to an optical photon flux, we need the material absorption coefficient α_{opt} for a given wavelength, and its optical power reflectance from the surface. The latter affects the net photon flux that reaches the active device surface, and therefore the boundary conditions. The former optical parameter, which is the absorption coefficient, is important to obtain the spatial distribution of the optical electron–hole generation rate. This may greatly affect the device performance, depending on whether the optical absorption occurs near a neutral region or a depletion region. The absorption coefficient of β-$FeSi_2$ is obtained from Ref. [18], and the fitting expression is shown as follows:

$$\alpha_{\mathrm{opt}}(h\nu)=3.82\times10^5(h\nu-E_{\mathrm{g}})^{1/2},\quad(2)$$

where E_{g} is the band gap of β-$FeSi_2$, and $h\nu$ is the energy of the absorbed photon. With a known absorption coefficient, the optical electron–hole generation rate used in the simulator is written as a function of distance y from the light entry point as follows:

$$G_{\mathrm{opt}}(y,h\nu)=\eta\frac{I_{\mathrm{opt_0}}}{h\nu}\alpha_{\mathrm{opt}}(h\nu)\exp[-\alpha_{\mathrm{opt}}(h\nu)y],\quad(3)$$

where $I_{\mathrm{opt_0}}$ is the light power intensity at the starting point inside the device, and η is the internal quantum efficiency.

Other models used in the simulator are Auger recombination, Shockley–Read–Hall (SRH) recombination, and interface and surface recombination. The Auger coefficient of β-$FeSi_2$ is estimated to be $C_{\mathrm{p}}=C_{\mathrm{n}}=1\times10^{-28}$ cm^6/s, and the lifetime of electrons and holes in β-$FeSi_2$ are estimated to be 1.0 μs.[21]

4. Simulation results and discussion

4.1. Effect of interface states

The origins of interface states are various and should be identified. The intrinsic interface states, resulting from mismatches in lattice and the thermal expansion coefficient, cannot be readily minimized. Practically, it is hard to maintain a low defect level by low-cost thin film processing technologies such as sputtering deposition, and so on. Note that different substrates can cause different lattice mismatches. A large mismatch can result in much more interface states. Therefore, one should take into account the influence of substrate orientation on interface states in the fabrication process, while the extrinsic interface states, such as Fe/Si non-stoichiometry, are the predominant cause for the imperfect interface between β-$FeSi_2$ and 4H-SiC layer.

In order to study the effect of defects, the surface recombination velocity is assumed to be 2×10^3 cm/s, which is not difficult to obtain by the passivation method. The density of the interface states for the p-type β-$FeSi_2$/n-type 4H-SiC heterojunction is presumed to change from 0 to 10^{13} cm^{-2}. The defect effects on the PD are simulated and the corresponding reverse dark current density (J_{RDC}) as a function of the reverse voltage for different interface states are shown in Fig. 3. It can be seen that J_{RDC} always increases when the density of interface states changes from 0 to 10^{13} cm^{-2}, and increases slightly

when the density of interface states is lower than 10^{10} cm^{-2}. After that, the J_{RDC} changes dramatically. The J_{RDC} does not saturate but increases monotonously with the reverse voltage. The results indicate that the recombination current in the β-$FeSi_2$ layer is dominant. Defects in the interface of the β-$FeSi_2$/SiC heterojunction may form a deep energy level in the band gap, which acts as an effective recombination center. Additionally, carriers tunneling through these defects at the interface can lead to the increase in J_{RDC}.[23]

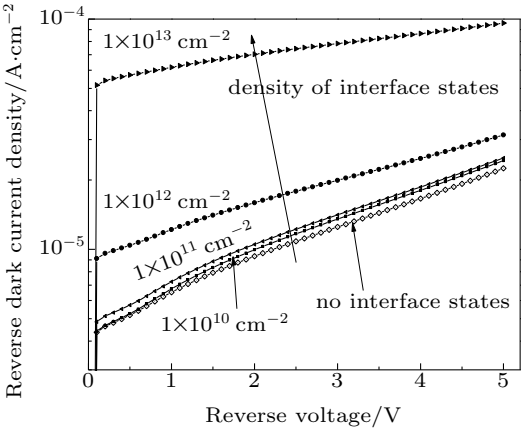


Fig. 3. Reverse current density versus reverse voltage for different interface states in the dark.

The photogeneration rate and recombination rate versus interface states are simulated under the illumination of a 6-mW (100 mW/cm^2) 1.31-μm laser at -1 V, as shown in Fig. 4. It can be seen that the recombination rate always increases with the increase in the interface state density, and the photogeneration rate is not affected by the interface states at the same light density. When the density of interface states is less than 10^{11} cm^{-2}, the maximum recombination rate via the interface is 1.38×10^{17} s^{-1}, which is much smaller than the photogeneration rate (2.32×10^{22} s^{-1}) in the β-$FeSi_2$/4H-SiC PD. While the density of interface states reaches 10^{14} cm^{-2}, the recombination rate via the interface reaches 1.28×10^{20} s^{-1}. In the range of the high density of interface state, the recombination rate is close to the generation rate, more and more photogenerated carriers disappear, and no longer contribute to the photocurrent, and then the photocurrent decreases significantly.

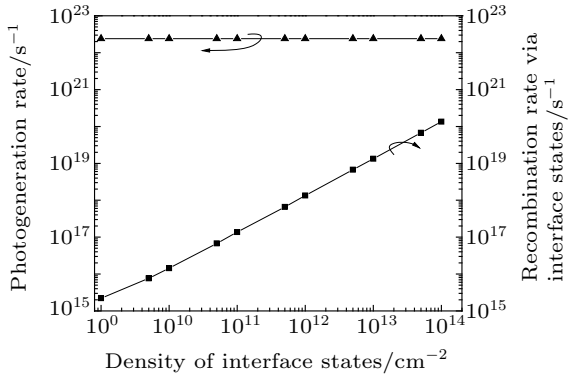


Fig. 4. Photogeneration rate and recombination rate versus interface states under illumination (100 mW/cm^2 at voltage of -1 V and $\lambda = 1.31$ μm).

It should be most suppressed by optimizing the process for the growth of the β-$FeSi_2$. Various optimization methods have been carried out in the past years, such as the thin template technique, the facing-targets direct-current sputtering method using lower substrate temperature without annealing, annealing process optimization, and surface passivating treatment. These methods aim to protect the PD from high interface states, and reduce the reverse leakage current of the β-$FeSi_2$/4H-SiC heterojunction.

4.2. *I–V* characteristics of the β-$FeSi_2$/4H-SiC hererojunction

In the above simulation, both surface recombination and interface states are considered. Although the interface states have an important impact on the device performance in the dark, the photocurrent is not markedly affected by lower interface states. Thus, in order to simulate the potential photoelectric characteristics of the β-$FeSi_2$/4H-SiC PD, the density of interface states (10^{11} cm^{-2}) is taken into account in the later simulation.

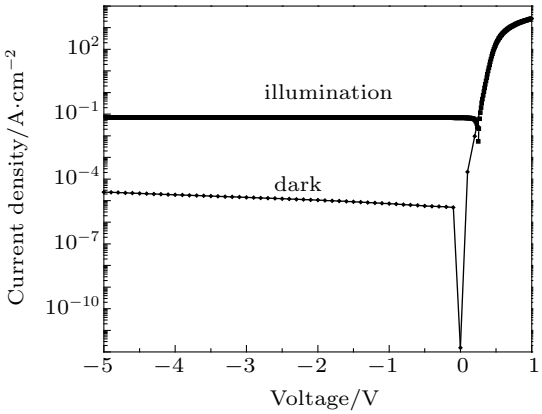


Fig. 5. *I–V* characteristics simulated in the dark and under illumination (100 mW/cm^2 at $\lambda = 1.31$ μm) at 300 K.

Figure 5 shows the *I–V* characteristics of the p-type β-$FeSi_2$/n-type 4H-SiC PD, simulated in the dark and under the illumination of the 6-mW (100 mW/cm^2) 1.31-μm laser at 300 K. The device exhibits good rectifying ability, which is similar to those of conventional p–n junctions. In the dark, the forward current at $+1$ V is approximately eight orders of magnitude greater than the reverse current at -1 V. The dark leakage current does not saturate but equal to 7.23×10^{-3} mA/cm^2 at a reverse voltage of -1 V, and this value increases slightly to 2.49×10^{-2} mA/ cm^2 at -5 V. This change may be caused by the interface states located in the band gap. The photocurrent at zero bias is 67.2 mA/cm^2, and this value reaches 69.7 mA/cm^2 and 70.3 mA/cm^2 at -1 V and -5 V, respectively. The ratio of the photocurrent to the dark leakage current at -1 V is about four orders of magnitude. The current responsivity at zero bias is estimated to be 67.2 mA/W. The open-circuit voltage (V_{oc}) and the short-circuit current density (J_{sc}) is about 250 mV and 67.2 mA/ cm^2, respectively.

4.3. Response of the β-$FeSi_2$/4H-SiC hererojunction

The related parameters, including doping and thickness of the p-type β-$FeSi_2$ layer, should play very important roles on the performance of the β-$FeSi_2$/4H-SiC PD, particularly with the p-type β-$FeSi_2$ layer as the main optical absorption layer due to its large optical absorption coefficient. In order to analyze their effects, the response is calculated for different doping levels and thicknesses. In the following, the bias voltage used in the simulation is -1 V, and the incident light is introduced to the device from the bottom, unless otherwise mentioned.

Figure 6 displays the spectral response under the reverse bias for different doping of the β-$FeSi_2$ layer. The results show that in the long wavelength range (> 1.55 μm), the spectral response is independent of the doping. While in the short wavelength range, the spectral response dramatically increases with the decrease in the doping concentration in the β-$FeSi_2$ layer, and the peaks red-shift in the NIR range. This effect results from the fact that the terminal of SCL in the p-side expands from the interface of β-$FeSi_2$/4H-SiC to the top, and more incident light with a longer wavelength can be absorbed within the SCL as it becomes wider. Therefore, considering the difficulty in lowering the doping, a doping concentration of the β-$FeSi_2$ layer should be chosen as 1×10^{15} cm^{-3}.

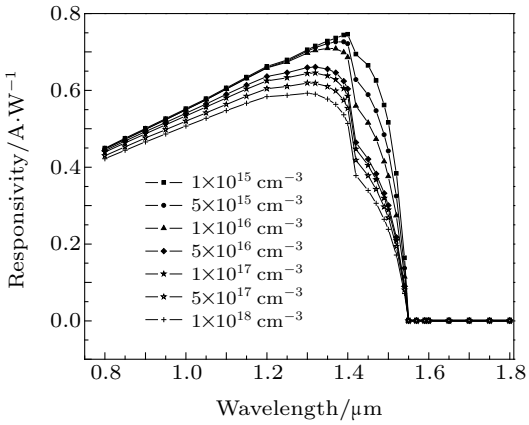


Fig. 6. The spectral response of the PD for different doping concentrations of the β-$FeSi_2$ layer at voltage of -1 V.

The spectral response of the β-$FeSi_2$/4H-SiC hererojunction for different absorption layer thickness is shown in Fig. 7. Within a range of layer thickness, which depends on the extension of the depletion layer and the diffusion length of minority carrier in the β-$FeSi_2$ layer, the response is a function of the β-$FeSi_2$ layer thickness. According to the simulation results, we find that the ideal thickness of the β-$FeSi_2$ layer is 2.5 μm, beyond which the thickness of the β-$FeSi_2$ layer has little effect on the photocurrent.

The photocarrier is generated mainly in the β-$FeSi_2$ layer, which can be seen from Fig. 8, where the photocarrier generation rates distribute over the entire device. These results show that the 4H-SiC epilayer almost has no absorption in the NIR range, while the β-$FeSi_2$ layer has strongly absorption, and the peak is located at the interface of the β-$FeSi_2$/4H-SiC hererojunction.

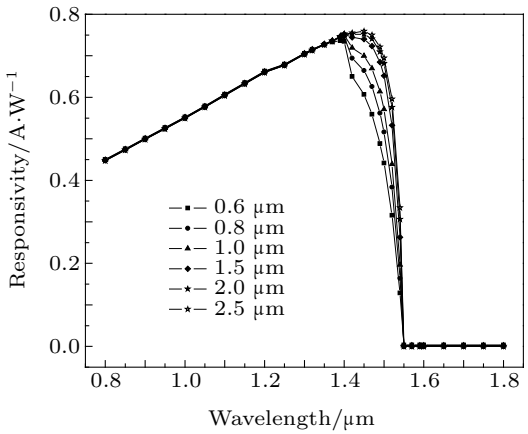


Fig. 7. The spectral response of the PD with different thickness of the β-$FeSi_2$ layer at voltage of -1 V.

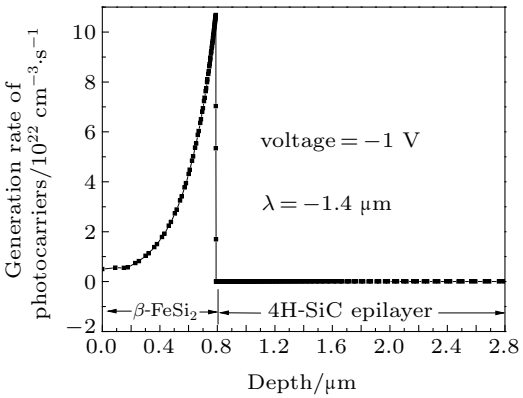


Fig. 8. Profiles of the photocarrier generation rate in the β-$FeSi_2$/4H-SiC heterojunction at voltage of -1 V and $\lambda = 1.4$ μm.

The spectral response of the β-$FeSi_2$/4H-SiC hererojunction for the propagation of the incident light is shown in Fig. 9. As the incident light enters from the bottom window of the cathode side, the response is two times higher than that for the injected light from the top window of the anode side. If the light is designed to enter the device from the anode side, the photocarriers cannot be fully attracted to the depletion layer due to the fact that the light is mainly absorbed near the front surface, not in the SCL near the interface of the β-$FeSi_2$/4H-SiC hererojunction. In short, while the light enters from the bottom window from the cathode side, higher responsivity can be obtained for the reverse bias voltage of -1 V at 300 K with a peak of 755 mA/W at 1.42 μm.

Based on the above analysis, a finally designed β-$FeSi_2$/4H-SiC hererojunction is composed of a p-type β-$FeSi_2$ layer with a thickness of 2.5 μm and a doping concentration of 1×10^{15} cm^{-3}, and a n-type 4H-SiC epilayer layer with a thickness of 2.0 μm and a doping concentration of 1×10^{16} cm^{-3}. Furthermore, a p-type β-$FeSi_2$/n-type 4H-SiC PD with a light window in the cathode side can achieve a higher spectral response in the NIR range.

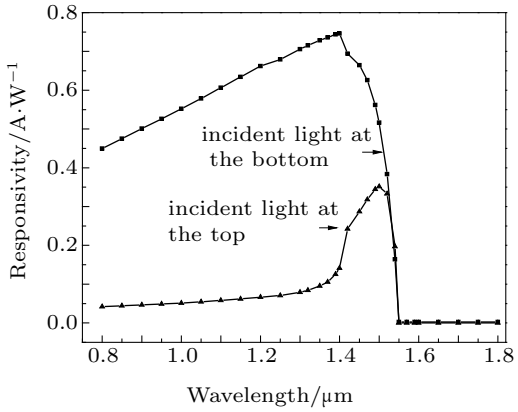


Fig. 9. Spectral response of β-$FeSi_2$/4H-SiC PD under different incident lights.

5. Conclusion

A novel NIR p-type β-$FeSi_2$/n-type 4H-SiC PD is proposed with semiconducting β-$FeSi_2$ as the active region. The PD has a good rectifying character and a good response to the NIR light. The interface states have an important impact on the device performance in the dark. However, the photocurrent is not markedly affected by higher interface states. The optimal value of the p-type β-$FeSi_2$ layer thickness and doping concentration is 2.5 μm and 1×10^{15} cm^{-3}, respectively, and an n-type 4H-SiC epilayer has a thickness of 2.0 μm and a doping concentration of 1×10^{16} cm^{-3}, respectively. The responsivity of the β-$FeSi_2$/4H-SiC detector with a light window in the cathode side can obtain a peak of 755 mA/W at 1.42 μm. These theoretical investigations enable us to better understand the inherent optoelectronic behavior of the β-$FeSi_2$/4H-SiC photodiode and can be utilized to optimize the device parameters for performance enhancement. We expect this structure to be applicable to NIR optically-activated SiC-based power switching devices.

References

[1] Geib K M, Mahan J E and Long R G 1991 *J. Appl. Phys.* **70** 1730
[2] Okajima K, Wen C, Ihara M, Sakata I and Yamada K 1999 *Jpn. J. Appl. Phys.* **38** 781
[3] Muduli P K, Herfort J, Schonherr H P and Ploog K H 2005 *J. Cryst. Growth.* **285** 514
[4] Akiyama K, Kadowaki T, Hirabayashi Y, Yoshimoto M, Funakubo H and Kaneko S 2011 *J. Cryst. Growth.* **316** 10
[5] Tan D, Chua C T, Dalapati G K and Chi D Z 2012 *Thin Solid Films* **520** 2336
[6] Okuda Y, Momose N, Takahashi M, Hashimoto Y and Ito K 2005 *Jpn. J. Appl. Phys.* **44** 6505
[7] Liu Z X, Osamura M, Ootsuka T, Kuroda R, Fukuzawa Y, Otogawa N, Nakayama Y, Makita Y and Tanoue H 2007 *J. Cryst. Growth.* **307** 82
[8] Herz K, Powalla M and Eicke A 1994 *Phys. Status Solidi A* **145** 415
[9] Shaban M, Nomoto K, Izumi S and Yoshitake T 2009 *Appl. Phys. Lett.* **94** 222113
[10] Shaban M, Izumi S, Nomoto K and Yoshitake T 2009 *Appl. Phys. Lett.* **95** 162102
[11] Li C, Yokoyama W, Izumi S, Nathaporn P and Yoshitake T 2010 *TENCON 2010 IEEE Region 10 Conference* November 21–24, 2010 Fukuoka, Japan, p. 2225
[12] Chen Z M, Pu H B and Fred R 2003 *Chin. Phys. Lett.* **20** 430
[13] Li L B, Chen Z M, Li T, Pu H B, Li Q M and Li J 2007 *Chin. Phys.* **16** 3470
[14] Li L B, Chen Z M and Yang Y 2011 *Mater. Lett.* **65** 1257
[15] Zhu F, Chen Z M, Li L B, Zhao S F and Lin T 2009 *Chin. Phys. B* **18** 4966
[16] Pu H B, Cao L, Chen Z M and Ren J 2011 *Chin. Phys. B* **20** 57304
[17] Danno K, Saitoh H, Seki A, Shirai T, Suzuki H, Bessho T, Kawai Y and Kimoto1 T 2012 *Appl. Phys. Express* **5** 031301
[18] Patrick H 2004 *ATLAS User's Manual* (9th edn.) (Santa Clara: SILVACO International) p. 36
[19] Gao Y, Liu H W, Lin Y and Shao G 2011 *Thin Solid Films* **519** 8490
[20] Ikeda M, Matsunami H and Tanaka T 1980 *Phys. Rev. B* **22** 2842
[21] Yuan J R, Shen H L, Lu L F, Huang H B and He X C 2010 *Physica B* **405** 4565
[22] Roschke M and Schwierz F 2001 *IEEE Trans. Electron Dev.* **48** 1442
[23] Yuan J R, Shen H L and Lu L F 2011 *Physica B* **406** 1733